Article

Integrating the PROSAIL and SVR Models to Facilitate the Inversion of Grassland Aboveground Biomass: A Case Study of Zoigê Plateau, China

Zhifei Wang [1,2] iD, **Li He** [1,2,]*, **Zhengwei He** [1,2], **Xueman Wang** [1,3], **Linlong Li** [1,3] iD, **Guichuan Kang** [1,3], **Wenqian Bai** [1,2] iD, **Xin Chen** [1,2], **Yang Zhao** [1,2] iD **and Yixian Xiao** [1,2]

1   State Key Laboratory of Geohazard Prevention and Geoenvironment Protection, Chengdu University of Technology, Chengdu 610059, China; wangzf@stu.cdut.edu.cn (Z.W.); hzw@cdut.edu.cn (Z.H.); wangxueman@stu.cdut.edu.cn (X.W.); 2021050068@stu.cdut.edu.cn (L.L.); kangguichuan@stu.cdut.edu.cn (G.K.); baiwenqian@stu.cdut.edu.cn (W.B.); chenxin_cx@stu.cdut.edu.cn (X.C.); zhaoyoung@stu.cdut.edu.cn (Y.Z.); xiaoyixian@stu.cdut.edu.cn (Y.X.)
2   College of Geography and Planning, Chengdu University of Technology, Chengdu 610059, China
3   College of Earth Sciences, Chengdu University of Technology, Chengdu 610059, China
*   Correspondence: heli2020@cdut.edu.cn

Abstract: Grasslands play a vital role in the global ecosystem. Efficient and reproducible methods for estimating the grassland aboveground biomass (AGB) are crucial for understanding grassland growth, promoting sustainable development, and assessing the carbon cycle. Currently, the available methods are limited by their computational inefficiency, model transfer, and sampling scale. Therefore, in this study, the estimation of grassland AGB over a large area was achieved by coupling the PROSAIL model with the support vector machine regression (SVR) method. The ill-posed inverse problem of the PROSAIL model was mitigated through kernel-based regularization using the SVR model. The Zoigê Plateau was used as the case study area, and the results demonstrated that the estimated biomass accurately reproduced the reference AGB map generated by zooming in on on-site measurements (R^2 = 0.64, RMSE = 43.52 g/m^2, RRMSE = 15.13%). The estimated AGB map also maintained a high fitting accuracy with field sampling data (R^2 = 0.69, RMSE = 44.07 g/m^2, RRMSE = 14.21%). Further, the generated time-series profiles of grass AGB for 2022 were consistent with the trends in local grass growth dynamics. The proposed method combines the advantages of the PROSAIL model and the regression algorithm, reduces the dependence on field sampling data, improves the universality and repeatability of grassland AGB estimation, and provides an efficient approach for grassland ecosystem construction and planning.

Keywords: aboveground biomass; PROSAIL; support vector machine regression; Zoigê Plateau

1. Introduction

Grassland ecosystems, as one of the most important ecosystems on Earth, are important for the maintenance of biodiversity, climate regulation, water resource management, and human economic and social development [1–3]. The aboveground biomass (AGB) of grassland, defined as the dry weight of the entire above-ground portion of a plant per unit area, is an important measure of the productivity of grassland ecosystems. It plays a decisive role in the healthy functioning of grassland ecosystems and is important for determining biosphere–atmosphere interactions [4–6]. The Tibetan Plateau is the most concentrated and largest area of alpine grasslands in the world. Its geography plays an important role in climate change on the Asian continent, making it a hotspot for the study of global climate change [7]. The Zoigê Plateau is located at the south-eastern edge of the Qinghai-Tibetan Plateau and contains alpine grassland and swampy meadows, which are representative of the grassland ecosystems of the Qinghai-Tibetan Plateau. It is also

an important water conservation area in the upper reaches of the Yangtze River and the Yellow River, playing an important role in the "Chinese Water Pagoda". It also occupies a pivotal position in China's national ecological protection and restoration projects [8,9]. Therefore, accurate assessment of the dynamic changes in the grassland AGB of the Zoigê Plateau is crucial for the sustainable development of grassland resources and ecosystem protection [10–12].

Traditional surveys of grassland resources are carried out by mowing the grassland. For field investigations, this approach can only be carried out on small areas of grassland and there is a certain degree of subjectivity in this approach. Further, this approach is time-consuming, labour-intensive, and can easily damage grassland resources [13–16]. With the development of remote sensing technology, satellite platforms with various spatial and temporal resolutions can provide relatively continuous data for monitoring the grassland biomass [1,17]. Remote sensing can achieve large-scale and long-term detection of grassland biomass through the optical characteristics of plants; this offers a unique and efficient method of estimation [18–20]. The study of grassland biomass using optical remote sensing data is more biased towards empirical estimation [13]. The available empirical estimation methods can be classified as parametric or non-parametric and include vegetation index regression [21,22], partial least squares regression (PLSR) [23,24], machine learning [15,25], and deep learning [26,27]. These are popular research methods as they are simple, intuitive, and easy to implement. However, empirical methods require a large amount of on-site measured data to calibrate the relationship between the remotely sensed data and the AGB. They also have obvious spatial and temporal limitations, affecting their versatility and portability [28]. Therefore, these empirical methods are difficult to apply to large-scale, long time-series, and specific growth period studies [29,30].

The canopy radiation transfer model (RTM) is a physical remote sensing method, based on physical principles and mathematical equations, that is used to explain the canopy's radiation transfer process [20,31]. Compared with empirical methods, physical models can better reflect complex surface environments, have high inversion accuracy, and show high adaptability in regions and grassland ecosystems with reduced data requirements [32–34]. The PROSAIL model, one of the major RTMs, has been widely applied to the inversion of biochemical variables and biophysical parameters of vegetation, such as the leaf area index (LAI) [35,36], leaf dry matter content (Cm) [37,38], and leaf chlorophyll content (Cab) [39,40]. Based on the characteristics of herbaceous plants, the grassland AGB can be expressed as the product of the leaf area index (LAI) and dry matter content (Cm) (AGB = LAI × Cm), and the LAI and Cm can be obtained by inversion of the PROSAIL model. Therefore, the PROSAIL model has been increasingly applied to grassland AGB estimation. For example, Quan et al. [20] used the PROSAIL model and Landsat-8 spectral data to invert the LAI and Cm to estimate the AGB. He et al. [30] estimated the grassland AGB in the Zoigê Plateau using the lookup table (LUT) method based on the PROSAIL model and MODIS products. However, due to the complexity of RTM, a large amount of computation is required to estimate grassland AGB, resulting in low efficiency. Therefore, some scholars have proposed the use of regression algorithms to estimate the biophysical parameters of grasslands. The introduction of regression methods into the estimation of the biophysical parameters of grasslands can effectively improve the accuracy and reliability of these estimates. For example, Oluseun et al. [36] combined PROSAIL and Gaussian process regression to estimate the phenological dynamics of the LAI of irrigated rice and achieved a more accurate estimation of the phenological dynamics. Jiao et al. [41] used the average leaf inclination angle of a specific crop as a priori input to estimate the canopy chlorophyll content of different crops based on the PROSAIL model and Random Forest regression algorithm. This approach effectively improved the inversion accuracy of canopy chlorophyll for wheat and soybean.

The SVR model [42], a nonlinear regression algorithm, can flexibly handle complex nonlinear patterns and has stronger expressive ability compared to some linear regression models. Due to errors in the PROSIAL model itself and the error between the model and

the actual data, different combinations of input parameters produce similar simulated reflectivity. This can lead to instability of the inversion results and reduced inversion accuracy. In contrast, the SVR model can be kernel-based regularised by setting the regularisation parameter and the relaxation variables in the formulae, so that the simulated training dataset built based on the PROSAIL model plays an active role in training SVR correctly and efficiently [43,44]. For example, Liang et al. [45] proposed an inversion method for the LAI of winter wheat using the NDVI, RVI, and four bands of blue, green, red, and near-infrared data as the input parameters for the SVR method. The results revealed that SVR estimation offers a better fitting effect and can make full use of the information contained in remote sensing bands to improve the accuracy of the remote sensing inversion of the LAI. Sawut et al. [46] estimated the betalain content using the PROSAIL and SVR model, and achieved a relatively high accuracy ($R^2 = 0.82$), indicating that the model is accurate and generalisable. These examples demonstrate that coupling PROSAIL and SVR can lead to better estimation of the biophysical parameters of grass. However, to date, few studies have used this inversion technique to estimate the AGB of grassland.

Therefore, this study coupled the advantages of the PROSAIL model and the SVR model, regularised the parameters of the SVR model, i.e., the penalty coefficient C and the slack variable ε, based on the RBF kernel, and selected the optimal hyper-parameters so as to achieve grassland AGB estimation with high accuracy and strong universal applicability. This study achieved the following three goals: (1) Forward inversion to create a simulated canopy spectral dataset based on Sobel global sensitivity analysis to recalibrate the ranges of grassland biophysical parameters that are input to the RPOSAIL model. (2) Estimation of the grassland AGB based on the simulated canopy spectral datasets trained on the SVR model. (3) Comparison of the estimated AGB with the reference AGB and the measured AGB, respectively, to verify its accuracy, and further analysis of intra-annual temporal variations in the AGB. This study meets the current needs of long series and large-scale estimation of grassland AGB and provides evidence for the accuracy and generalisability of estimating the grassland AGB based on the RTM and regression algorithms.

2. Materials and Methods

2.1. Region of Interest

The Zoigê plateau is located in the south-eastern margin of the Tibetan Plateau (between 31°48′4″~34°48′28″, 100°47′35″~103°39′37″) at an altitude of 3000 to 4500 masl. The Zoigê plateau is a representative area of the grassland ecosystems of the Qinghai-Tibetan Plateau; it is also an important water conservation area upstream of the Yangtze River and Yellow River [47]. The ecological security of the Zoigê plateau's rich grassland and wetland resources is related to the socio-economic development of the western region, the Yellow River Basin, and the Yangtze River Basin. From the perspective of geographical and administrative regions, it involves Aba County, Zoigê County, and Hongyuan County of Sichuan Province and Maqu County and Luqu County of Gansu Province. It occupies a total area of 44,758 km² (Figure 1). The average annual temperature is approximately 0–2 °C, and the average annual precipitation is approximately 600–800 mm [48].
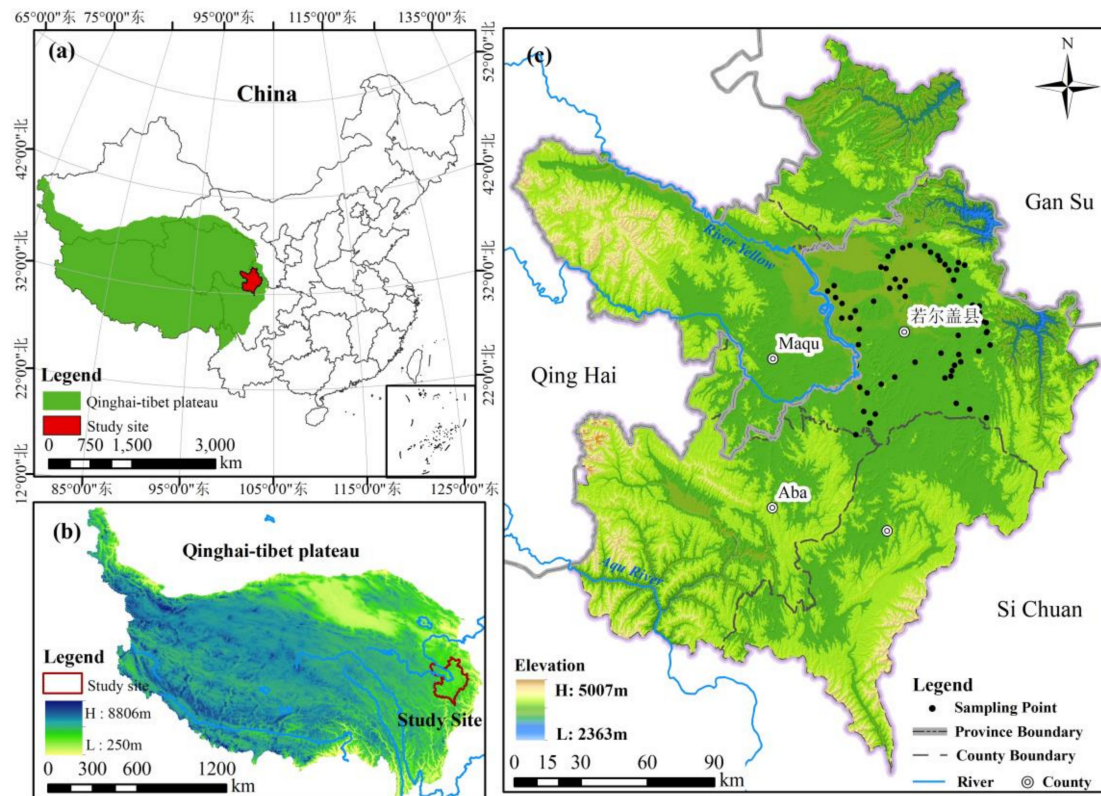
Figure 1. Zoigê Plateau topography and sampling point distribution. (**a**) Location of the study area within China; (**b**) the study area on the Qinghai-Tibet Plateau; (**c**) topography and administrative regions.

2.2. Datasets

2.2.1. Field Measurements and Reference AGB Map

Grassland data were collected from the study area from 18–23 August 2022 during the peak growing season. The sample plots were chosen based on the representativeness of vegetation cover and type distribution. Sample plots of 61 100 × 100 m were set up in the study area and their geographical coordinates (latitude, longitude, and elevation) were recorded in detail using GPS. The plots were randomly sampled three times with sample squares of 0.2 × 0.2 m. The above-ground parts of the grass in these sample squares were completely clipped off. Impurities were removed from the grass samples, and they were transported to the laboratory in sealed sample bags. The samples were then dried in an air-drying oven at 80 °C for 48 h until a constant dry weight was obtained. The grass samples from each plot were weighed and averaged to measure the AGB for that plot. Yin et al. [11] used Landsat 8 OLI data and the Consistent Adjustment of Climatology and Actual Observations (CACAO) method combined with Gaussian Process Regression (GPR) to generate a seamless AGB map from sparse field measurements; this served as the reference AGB.

2.2.2. MODIS Reflectance Data Collection

The MCD43A4 ground reflectance dataset generated by the MODIS satellite sensors on board the Terra and Aqua satellites was selected to estimate the grass LAI and Cm, which were multiplied to obtain the AGB. The MCD43A4 images provide daily reflectance data over a distance of 500 m, and this data contains seven bands. The data were obtained from EARTHDATA (https://www.earthdata.nasa.gov/ (accessed on 11 April 2023)). The cloudiness of the selected data was less than 5%.

2.3. Research Methods

Based on the characteristics of herbaceous plants, the physical method of estimating the AGB of grassland by coupling the PROSAIL model with SVR can be expressed as the product of Cm and LAI, both of which are used as input parameters to the PROSAIL model. A Sobel global sensitivity analysis was first performed on the parameters input to the PROSAIL model to determine their step or fixed values. Based on this, forward inversion was performed to obtain a simulated canopy spectral dataset covering the 400–2500 nm band. The continuous spectra were filtered using the Popper response function of MODIS, converted to pixel spectra of MCD43A4, and combined with the AGB (LAI × Cm) to create a simulated training dataset. The SVR model was trained based on the training data and the optimal hyperparameters were selected for the regularisation parameters and relaxation variables in the model. Then, the grassland AGB in the study area was estimated using the MCD43A4 surface reflectance as input data. Finally, the estimated and reference AGBs were compared with the measured AGBs to verify their accuracy, and the time variations were analysed. Figure 2 shows the workflow of this study.
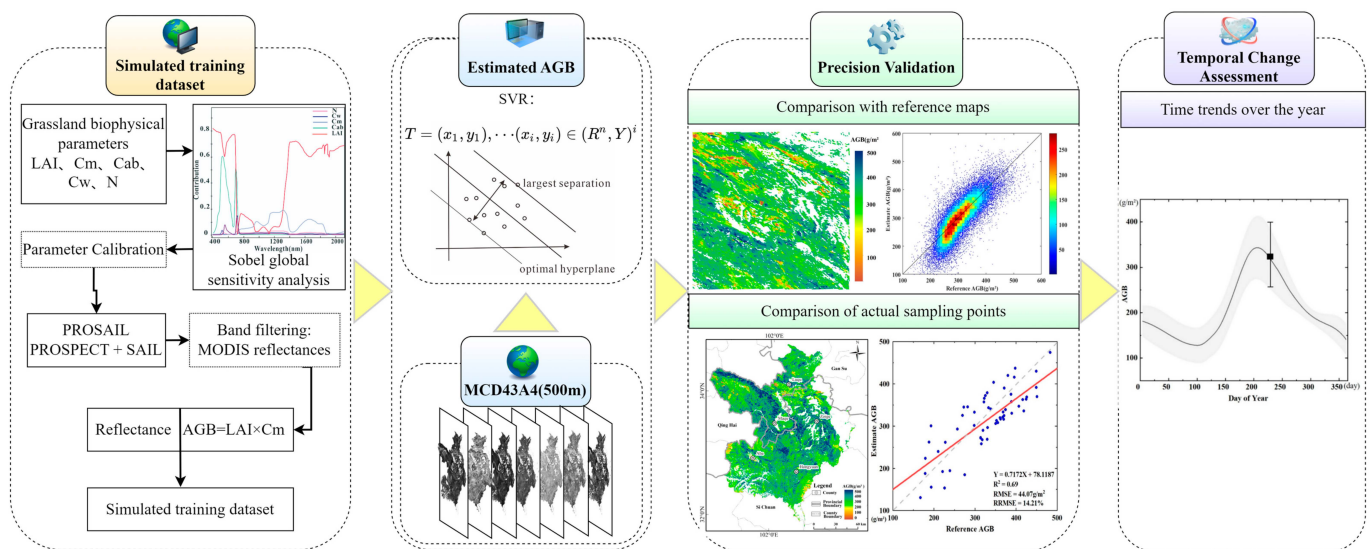

Figure 2. An overview of the study design for the four aspects of this study: (1) creation of simulation training datasets; (2) estimation of the grassland AGB; (3) comparison of the accuracy of the estimated AGB with the reference AGB and measured AGB; (4) temporal change assessment.

2.3.1. PROSAIL Model

The PROSAIL model is a commonly used vegetation RTM used to model vegetation spectral characteristics and radiative reflectance; it establishes a clear physical relationship between vegetation biophysical parameters and remote sensing observations [49]. It combines two classical vegetation spectral models, the PROSPECT model [50] and the SAILH model [51]. The PROSPECT model is a spectral model whose input parameters are leaf structural parameters (N), water content (Cw), chlorophyll content (Cab), carotenoid content (Car), browning pigment content (Cbq), dry matter content (Cm), etc. It is capable of describing the interactions between light and plant leaves with high quality using a small number of input parameters and can simulate the spectral characteristics of different leaves. The PROSPECT model equation is shown in Equation (1) (version PROSPECT-5B) [52]. The calculated leaf reflectance and leaf transmittance, combined with parameters such as the LAI, hotspot effect (hotspot), soil factor (psoil), mean leaf inclination (LIDFa), observed zenith angle (tto), solar zenith angle (tts), and relative azimuthal angle (psi) are then en-

tered into the SAILH model to obtain the canopy reflectance ρ_c, as shown in Equation (2) (Version 4SAIL) [53].

$$(\rho_i, \tau_i) = \text{PROSPECT}(N, Cab, Cw, Cm, Car, Cbp), \qquad (1)$$

$$\rho_c = \text{SAILH}(LAI, hspot, psoil, LIDFa, tto, tts, psi, \rho_i, \tau_i). \qquad (2)$$

The input parameters, descriptions, ranges, and standard values required for the PROSAIL model are shown in Table 1.

The input data for the PROSAIL model includes all the parameters of the SAILH and PROSPECT models. Thus, this involves a large number of parameters, redundant calculations, and is prone to excessive data volume. This is not conducive to accurate and efficient inversion. In previous studies where PROSAIL was used to invert the biophysical parameters, the input parameters were mainly determined based on the biophysical data of the canopy obtained from existing databases, and the results obtained using these parameters could not be directly used for studies of different regions due to regional differences. Therefore, it is necessary to conduct sensitivity analyses of these parameters to determine their contributions to specific bands, with the aim of reducing the computational complexity of the model and ensuring the accuracy of the simulated spectra.

Sensitivity analysis can be classified as local sensitivity analysis or global sensitivity analysis. Local sensitivity analysis ignores the effect of changes in other parameters by fixing them, and the contributions of each parameter are not accurately described. Global sensitivity analysis can avoid the shortcomings of local sensitivity analysis by calculating the changes in all of the model parameters and then obtaining the contribution of each parameter to the model. Sobel global sensitivity analysis is an application of the Monte Carlo method of sampling. It can be used to effectively explore the effects of each parameter on the model simulation results themselves [54]. Therefore, this study adopted variance-based Sobel global sensitivity analysis to rank the sensitivity of the input parameters (Cm, Cw, LAI, Cab, and N). Based on the idea of model decomposition, the sensitivity of the parameters can be analysed once, twice, or more to prevent the impact of insufficient samples and uneven distributions on the sensitivity analysis. Based on the PROSAIL model, the five parameters were sampled 10,000 times and their global sensitivity was calculated. We then analysed the sensitivity of each parameter in the range of the band.

Table 1. Input parameters required by the PROSAIL model.

Model	Parameter	Symbol	Range	Standard	Source
PROSPECT_5B	Chlorophyll content	Cab	5~100 µg/cm^2	40	Xu et al. [55]
	Leaf structure parameter	N	1~2	1.25	Feilhauer et al. [56]
	Carotenoid content	Car	8		Model default
	Leaf brown pigment	Cbrown	0		Model default
	Dry matter content	Cm	0.001~0.01 g/cm^2	0.005	Si et al. [34]
	Leaf water content	Cw	0.003~0.03 g/cm^2	0.0125	Liang et al. [57]
4SAIL	Leaf area index	LAI	0.1~8	2	Si et al. [34]
	Hot spot factor	Hspot	0.05~1	0.075	He et al. [32]
	Soil moisture ratio	Psoil	0.5~1	0.1	Huang et al. [58]
	Zenith angle	θs	0~90°	20°	He et al. [32]
	observed azimuth angle	θv	0~90°	0	Li et al. [59]
	Leaf inclination	LIDFa	30		Model default
	Leaf distribution	LIDFb	0		Model default

2.3.2. Grassland AGB Inversion Based on SVR Modelling

In this study, the SVR model was used to perform grassland AGB inversion, with the MCD43A4 ground reflectance data as the feature variables. SVR is a generalisation of SVM for regression applications. It is based on the construction of a hyperplane (or

multiple hyperplanes). It minimises the error between all training samples and the optimal hyperplane by searching for the optimal classification surface. It can handle linear and nonlinear regression fitting problems [60]. It can be expressed as follows:

$$T = \{(x_1, y_1), \cdots (x_i, y_i)\} \in (R^n \times Y)^i,$$ (3)

where x_i is the input variable, y_i is the output variable and R is the set of real numbers. Similar to the classification problem, the possible values of y are inferred from the training set based on the value of x, where y can take any value.

Compared to other models, SVR models can achieve kernel-based regularisation by controlling the penalty coefficients and the slack variables; thus, SVRs are relatively robust to noise and outliers. This can help to balance the complexity and fit of the training dataset. SVR models fit the data by minimising the data points in the intervals, which makes them less susceptible to noise and outliers. When dealing with nonlinear problems, kernel functions are required to map the input training samples to the higher dimensional space, which helps in dealing with complex relationships [61,62]. In this research, the RBF was used as the kernel function of the SVM. Considering the performance of the model, three main parameters were selected during the training process: the kernel function hyperparameter (gamma), penalty coefficient (C), and slack variable (epsilon), which were set to 0.23, 4.7, and 0.15, respectively. Since the modelled output covariates of the SVR model are not affected by multicollinearity, all seven reflectance bands of the simulation were chosen to participate in the modelling.

2.3.3. Model Validation

To evaluate the performance of the research method in estimating the AGB in this study, the trained and hyperparameter-optimized SVR model was applied to MCD43A4 images, and the reference AGB map and on-site measured values were used for evaluation. The reference AGB map measured in the enlarged field was aggregated to the same spatial resolution as the MCD43A4 surface reflectance product. The accuracy of estimating the AGB was evaluated using the coefficient of determination (R^2), root mean square error (RMSE) and relative root mean square error (RRMSE). The evaluation indicators were calculated as follows (Equations (4)–(6)).

$$R^2 = 1 - \frac{\sum_{i=1}^n \left(y_{mean} - y_{est}\right)^2}{\sum_{i=1}^n \left(y_{mean} - \overline{y}_{mean}\right)^2},$$ (4)

$$RMSE = \sqrt{\frac{\sum_{i=1}^n \left(y_{est} - y_{mean}\right)^2}{n}},$$ (5)

$$RRMSE = \sqrt{\frac{\sum_{i=1}^n \left(y_{est} - y_{mean}\right)^2}{n}} \times \frac{100}{\overline{y}_{mean}},$$ (6)

where y_{est} is the estimated AGB, y_{mean} and $\overline{y}_{mean}$ are the measured AGB and the average value of the measured AGB, respectively, and n represents the number of on-site survey points.

Then, a temporal dynamic analysis was conducted on the estimation results. Based on the time series of surface reflectance of MCD43A4, the AGB of the study area covering days 1–365 in 2022 was estimated, and a time profile was generated to check whether the estimated AGB can adapt to the dynamic changes in grassland phenology. Further, the performance of this method was evaluated.

3. Results

3.1. Recalibration of the PROSAIL_5B Model Parameters

By analysing the global sensitivity of each parameter using Sobel's algorithm, the global sensitivity curves of each parameter were obtained (Figure 3).
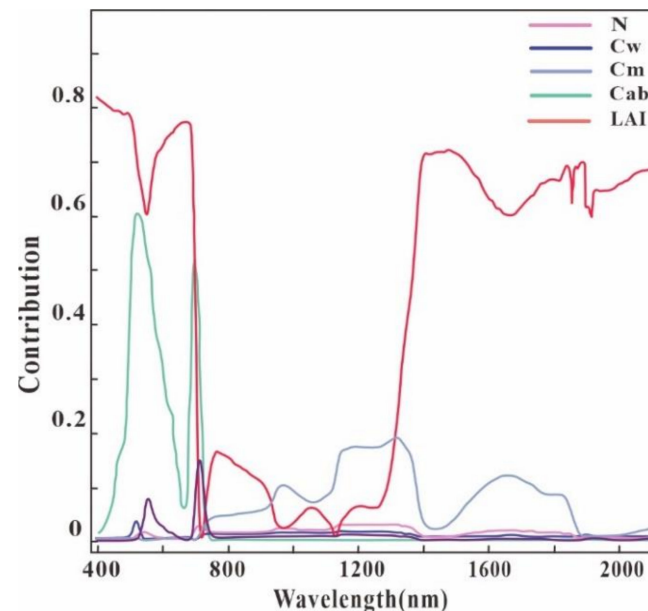

Figure 3. Sobel global sensitivity analysis results.

As can be seen, the global sensitivity of Cab exhibited a large amplitude of change, varying between 0 and 0.6, with the main fluctuation within the 400–780 nm range and a peak value of about 0.6. It then dropped sharply with a trough value of about 0.05. The global sensitivity of Cw exhibited a small amplitude of change, with a high contribution in the visible wavelengths; its contribution was 0 within the range of 760–2400 nm. When the contribution was 0, the global sensitivity of Cm exhibited a larger variation, with obvious changes between 0 and 0.23. There was also an obvious downward trend near the 1350 nm band, followed by a rise to a peak. The global sensitivity of LAI also exhibited a larger variation between 0.1 and 0.95, with an obvious peak and trough near the 760 nm wavelength. The N global sensitivity did not exhibit large variation; it was relatively stable in the range of 400 nm to 2400 nm, with variations between 0 and 0.03; the greatest influence was in the near-infrared wavelength band (Figure 3).

Based on the above analysis, it is found that the parameters, three parameters, LAI, Cab, and Cm, had the greatest influence on the reflectance of the grass canopy. Thus, they were input into the PROSAIL model at certain step changes and were ultimately set to a smaller step to improve the accuracy of the data. The other two parameters, N and Cw, which were less sensitive, were fixed to a set value that was determined based on several model optimisation simulations and consultation with references. Other values, such as the hotspot size, zenith angle, observation azimuth, and soil factor, were set to fixed values based on experience and consultation with references (Table 1). Ultimately, 10 parameters were calibrated (Table 2). Based on the above, the calibrated parameter values, which were fixed or step values, were input into the PROSAIL model for inversion. A total of 96,000 simulated spectra and corresponding parameter combinations were generated for subsequent SVR model training.

Table 2. Recalibration of input parameters for the PROSAIL 5B model.

Parameter	Symbol	Range	Step Size
Chlorophyll content	Cab	5~100 µg/cm^2	5
Leaf structure parameter	N	1.7	-
Azimuth angle	θv	0°	-
Solar zenith angle	θs	20°	
Soil factor	Psoil	0.5~1	0.1
Dry matter content	Cm	0.001~0.01 g/cm^2	0.001
Leaf water content	Cw	0.015 g/cm^2	-
Leaf area index	LAI	0.1~8	0.1
Hot spot factor	Hspot	0.075	-
Average leaf inclination angle	LIDFa	20.2°	-

3.2. Verification of the AGB Estimation Accuracy

The recalibrated parameters in Table 2 were input into the PROSAIL model for inversion. Then, the MODIS Popper response function and the input parameters LAI and Cm were used to calculate the grassland AGB. Next, 96,000 simulated training sets were constructed to train the SVR model, and the AGB was estimated by the optimal selection of hyperparameters and was verified in terms of accuracy.

Based on the SVR model, the spatial distribution of the grassland AGB was generated on day 225 of 2017 for the same study area as analysed by Yin et al. (Figure 4a). The two spatial distributions were compared by extracting the same pixel points and plotting a scatter plot (Figure 4b). The results showed that the points were distributed near the 1:1 contour line and were mainly concentrated between 100 and 500 g/m^2, with an R^2 of 0.64, an RMSE of 43.52 g/m^2, and an RRMSE of 15.13%. At AGB values between 200 and 300 g/m^2, there was slight underestimation, but no overestimation. There was also high similarity and a clear trend in the spatial distribution maps of the two, specifically, there were higher AGB values in areas close to the river, as compared to areas away from the river. It is worth noting that the reference map per se is also uncertain.
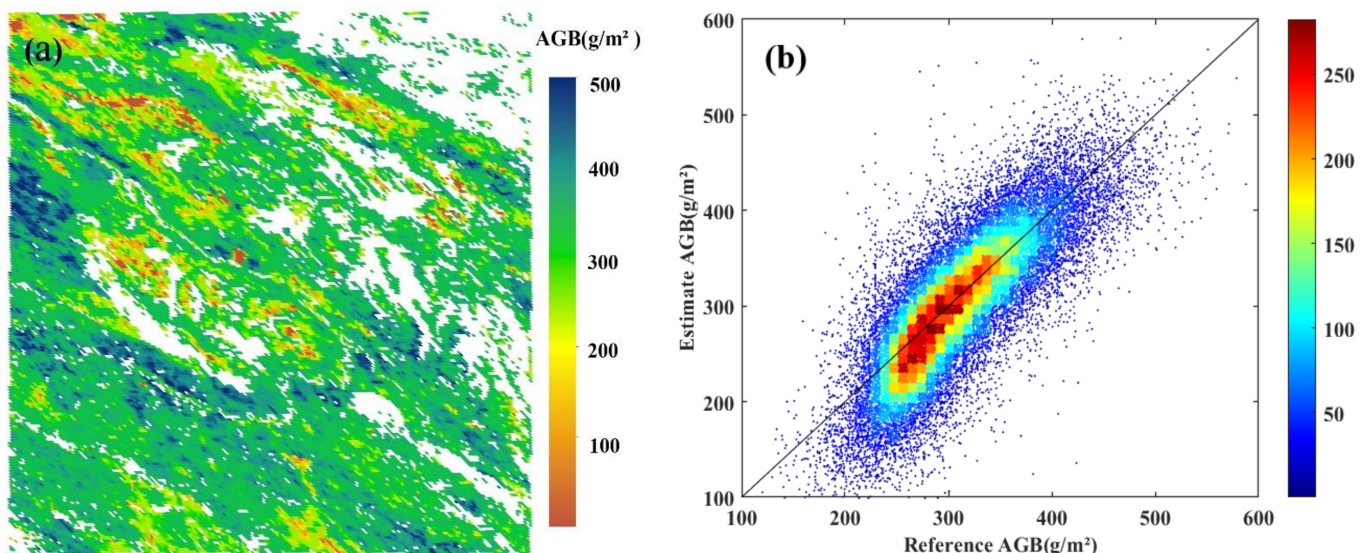

Figure 4. Direct pixel-by-pixel comparison between the reference and estimated AGBs on day 225, 2017. (**a**) Grassland AGB map generated based on estimated (the white pixels in (**a**,**b**) are bad pixels and non-grass pixels). (**b**) Density scatterplots between the estimated AGB and reference AGB.

In addition, the spatial distribution map of the average AGB of the grassland within the study area from 18 to 23 August 2022 was drawn using the SVR model (Figure 5);

the non-grassland parts (the white parts in Figure 5: forests, rivers, built-up land, etc.) were excluded. The spatial distribution of the AGB of the Zoigê Plateau grassland can be seen to be heterogeneous, with a gradual increasing trend from the north-western to the southeastern direction. The sampling points were projected into the raster image and the corresponding pixel values were extracted to establish a linear fitting relationship with the measured grassland AGB (Figure 6). It was found that using the methodology developed in this paper, there was a good fit between the estimated grassland AGB and the measured AGB, with an R^2 of 0.69, an RMSE of 44.07 g/m^2, and an RRMSE of 14.21%. However, the AGB values were partially underestimated in the range of 200–300 g/m^2, which is consistent with the results of the above comparison with the reference AGB. These findings further validate the estimation accuracy of our method.
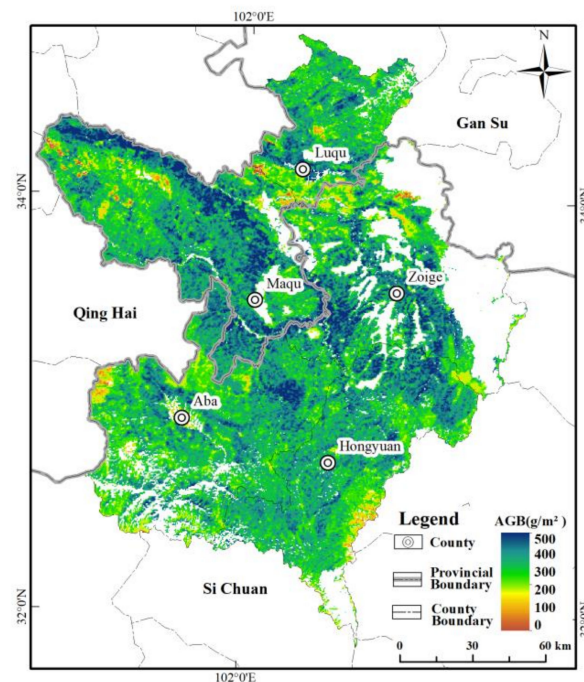

Figure 5. Spatial distribution of the grassland AGB in the Zoigê plateau on day 230 of 2022 estimated from the SVR model.
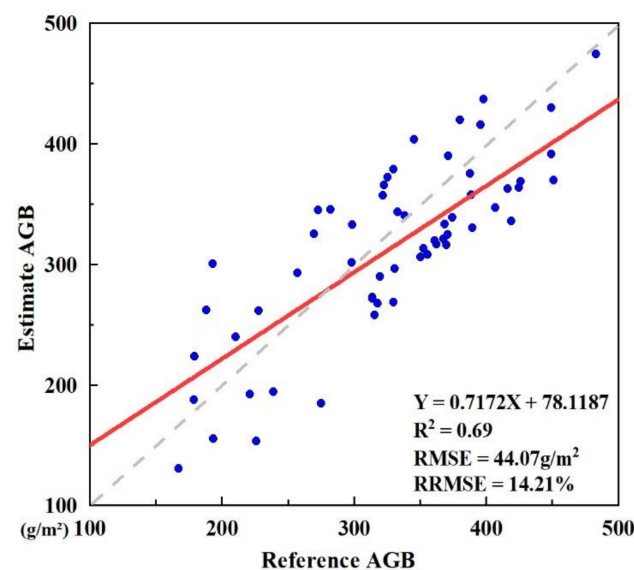

Figure 6. Relationship between the field-measured and estimated AGB. The Blue dots indicate sampling points, solid line represents the fitted regression line, and the dashed line represents the 1:1 line.

3.3. Time-Dynamic Analysis

The trained SVR model was used to estimate the AGB time variation image covering the study area from 1 to 365 days in 2022. The time distribution of the AGB values corresponds to the time of downloading the MCD43A4 reflectance products, and its standard deviation was calculated, as shown in Figure 7. From the graph, it can be seen that the estimated AGB time series offered a satisfactory reproduction of the dynamic trend in the grassland phenology. The grassland growth season occurred from 105 to 315 days and reached its peak on the 203rd day, with an average value of 358.578 g/m^2. When the grassland was in a dormant state, the grassland AGB values still exhibited a downward trend and were not zero, which may be related to winter and summer pastures. During winter, the research area is still covered with a large amount of dry grass for livestock breeding [63,64].
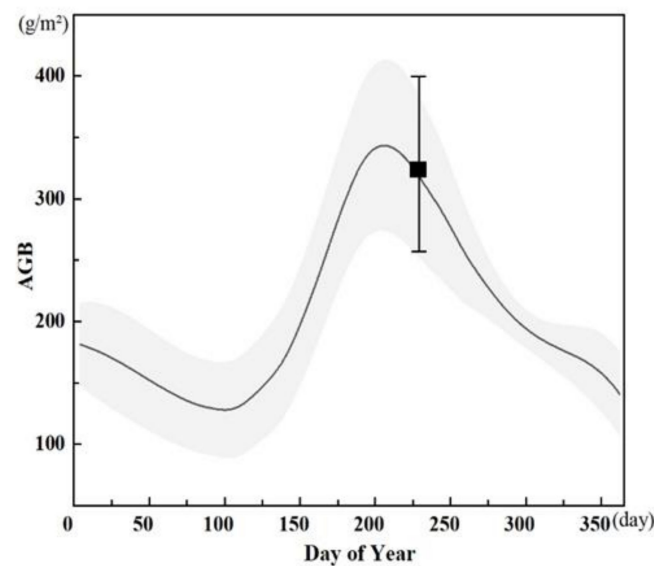

Figure 7. Temporal profile of the estimated AGB in our study area for days 1 to 365 days in 2022. (the shaded area represents the standard deviation of the estimated AGB. The mean and standard deviation of the reference map are displayed as a solid box and corresponding error bars).

4. Discussion

4.1. Advantages of Our Grassland AGB Estimation Scheme

The traditional AGB estimation method for grassland relies on the empirical relationship between field-measured data and remotely sensed vegetation indices. This method is relatively mature and is still widely used in research. For example, Yang et al. [55] constructed an artificial neural network model based on a large amount of field measurement data and selected five optimally correlated variables out of 13 variables, with correlations of 0.75–0.85. Zeng et al. [29] used a Random Forest algorithm to estimate grassland AGB by experimentally comparing five variables selected with a corresponding R^2 of 0.86. These studies required a large amount of on-site measurement data, and the on-site measurement data were not fully representative. These methods have certain temporal and regional specificity and cannot describe the seasonal changes in vegetation; they also have low repeatability and are difficult to apply widely. The current study proposed a physical method of combining the PROSAIL model with the SVR model to estimate grassland AGB using MCD43A4 surface reflectance images. This method was able to achieve continuous spatiotemporal estimation of grassland AGB on the Zoigê Plateau in the absence of measured data, with good estimation accuracy. At the same time, our method has the obvious advantage of producing continuous spatio-temporal grassland AGB values with better repeatability and adaptability than traditional methods because it does not require ground

measurements. Its ability to provide low-cost and large-scale grassland monitoring is also a strength of this method.

The existing methods for estimating grassland AGB based on RTM rely more on the LUT method, which is relatively computationally intensive and inefficient and requires regularization strategies to alleviate the drawbacks of ill-posedness. For example, He et al. [32] used the PROSAIL model and the LUT method to invert MCD43A4 images with limited accuracy (RMSE and RRMSE of 60.06 g·m^{-2} and 18.1%, respectively); there was both underestimation and overestimation of the AGB values when the reference value was less than 200 g/m^2 and between 300 and 350 g/m^2. Quan et al. [20] estimated grassland AGB based on the PROSAIL model and LUT and compared the results with those obtained using exponential regression, partial least squares regression, and artificial neural networks. The authors found that the former had better accuracy (R^2 = 0.64, RMSE = 42.67 gm^{-2}). Compared with the LUT method, we estimated the grassland AGB by SVR, which reduced the calculation complexity and improved the efficiency and accuracy of estimation (R^2 of 0.69, RMSE of 44.07 g/m^2, RRMSE of 14.21%). The PROSAIL model assumes that the dry matter content is only present in the leaf structure when modeling the grass AGB, ignoring the effect of the stem; this leads to a lower estimate than the reference value when the reference value is between 200 and 300 g/m^2, but not an overestimation. Thus, our results are more interpretable.

Due to the complexity of the RTM, new methods that combine the RTM and regression models have been proposed and are now more commonly used in the inversion of grassland biophysical parameters. However, they have rarely been used in research estimating grassland AGB maps [46,65]. Further, in the study by Durbha et al. [44], which used the PROSAIL model and SVR model to estimate the LAI from a multi-angle imaging spectrometer, it was found that when using the canopy reflectance model to invert biophysical variables, different input parameter combinations and values in the RTM may lead to similar reflectance due to model errors and deficiencies between the model and the actual situation. This may lead to instability and uncertainty in the estimation results. Kernel-based regularisation using the SVR method can address this problem. However, this method has not been validated for the estimation of grassland AGB. Therefore, in this study, our proposed method using the PROSAIL model combined with the SVR model performed RBF kernel-based regularisation by setting the regularisation parameters, i.e., the penalty coefficient C and the relaxation variable epsilon, as a way to reduce the error of the PROSAIL model itself as well as the error between the canopy spectral dataset in which the model is inverted and the actual values. Since we improved the rationality of the input parameters of the PROSAIL model reduced the noise in the training dataset and optimally selected the hyperparameters of the SVR model, our study is significantly more accurate than Zhang et al. [62]'s estimation of grassland AGB by combining the PROSAIL model with the SVR model based on the LUT algorithm (R^2 = 0.30, RMSE = 32.88 g/m^2, RRMSE = 41.94%). Therefore, the estimation of grassland AGB by coupling the PROSAIL model and SVR method is more reproducible and robust, and this method has significant prospects for future development.

4.2. Spatial and Temporal Dynamics of Grassland AGB in the Zoigê Plateau

In this study, the spatial distribution of the mean grassland AGB from 18–23 August 2022 (Figure 5) and the time series of grassland AGB from day 1 to 365 (Figure 7) on the Zoigê Plateau were plotted, respectively, using our methodology. In terms of space, the grassland AGB map of the Zoigê Plateau in 2022 exhibited significant heterogeneity in its spatial distribution, showing a gradual increasing trend from the northwest to southeast. This may be related to the altitude and geographical environment of the Zoigê Plateau. The eastern region has a lower altitude and abundant wetlands, which are relatively more suitable for the growth of grasslands. From Figure 5, it can be seen that areas with abundant water resources had higher grassland AGB values. In the time series, the growing season appeared from day 105 to 315, peaked at day 203, and declined from day 315 until day 105 of the next year, which is the grass dormant period. From Figure 7, it can be seen that the

AGB was not 0 in the grass dormant period, and there was a certain downward trend. This is because, in winter, herders store a large amount of hay for livestock consumption; thus, in the dormant period, the grass AGB is not zero [64]. The reason for the decreasing trend may be because the grass consumed during grazing is greater than the average carrying capacity of the plateau during the dormant period [66,67]. In summary, the grass AGB estimation method developed in this paper provides a good reflection of the trends in climatic change and the spatial characteristics of the grassland AGB in the Zoigê Plateau. This method is not restricted to a specific time and region, offering a more robust and universal estimation method than empirical methods.

4.3. Factors Affecting the Accuracy of Grassland AGB Estimates

There are still some uncertainties with our research methods. Findings, the grassland AGB value estimated by coupling the PROSAIL model and SVR model was lower than the reference value between 200 and 300 g/m^2 (Figures 4b and 5). In addition to ignoring the influence of roots and stems, it is also possible that the soil parameters we set may not be consistent with the actual soil properties of the grassland in the Zoigê Plateau, resulting in underestimation. Therefore, in future-forward inversions of the PROSAIL model, the soil parameters should be revised to improve estimation accuracy. Further, the research method in this paper is based on the MODIS sensor surface reflectance product MCD43A4, which has a resolution of 500 m, while the real measurements were performed at 100 m. This may have led to scale errors in the comparisons and may have affected the accuracy of the estimation results. Nonetheless, with the remote sensing technology and improved data quality, our method may obtain better estimation results than those obtained with traditional methods, and our method has better portability and robustness. Moreover, in this study, the grassland AGB was estimated by establishing biophysical parameters for grassland, which makes the model only applicable to the inversion of grassland AGB. The Zoigê Plateau has a diversity of species and vegetation types such as forests and scrubs, which is also a reason for the underestimation of the AGB values. In future research, the PROSAIL model should use a more representative spectral library for grassland soil collection [68] to improve the setting of soil parameters. Moreover, the use of high-resolution images, such as Landsat and Sentinel data, would help to keep the image resolution as consistent as possible with the resolution of on-site measurements, to improve the accuracy of grassland AGB estimation.

It Is worth noting that different machine learning models may yield better results, and coupling as many machine learning models as possible with the PROSAIL model and exploring their AGB estimation results would provide a meaningful extension to this study. In addition to this, human activities such as fencing and grazing may also have impacts on the estimation of grassland AGB. Quantifying the spatial and temporal impacts of human activities and incorporating them into the model for regionalised AGB estimation and comparison in subsequent studies is worth pursuing, especially for different grassland types on a global scale.

5. Conclusions

This study demonstrates the potential of coupled PROSAIL and SVR models for grassland AGB physical inversion. The developed method combines the advantages of both models, greatly reducing the computational complexity of the estimation process and providing reliable estimation accuracy. The method relies on the characteristics of herbaceous plants and reduces the AGB to the product of LAI and Cm, both of which are used as inputs to the PROSAIL model. The parameters are inverted by redetermining the range and step values of the input parameters of the PROSAIL model based on Sobel global sensitivity analysis. The resulting simulated training dataset is inverted, and regularisation based on RBF kernels is performed using the SVR model in order to estimate the grassland AGB. This method performs well against both measured AGB values and reference AGB values. The utility of the method was highlighted in the assessment of the spatial and seasonal variation in the grassland AGB. Satisfactory trends in phenology were reproduced

by estimating the grassland AGB time series for 2022. Ultimately, these findings contribute to effective continuous spatiotemporal monitoring of the regional grassland AGB and provide alternative methods for research in other regions worldwide.

Author Contributions: Conceptualization, L.H. and Z.H.; methodology, L.H.; software, L.L. and Z.W.; validation, Z.W., Y.X. and G.K.; formal analysis, W.B.; investigation, X.C.; writing—original draft preparation, Z.W.; writing—review and editing, X.W.; visualization, Y.Z. All authors have read and agreed to the published version of the manuscript.

Data Availability Statement: The satellite products were downloaded from: https://ladsweb.modaps.eosdis.nasa.gov/ (accessed on 11 April 2023). MODIS spectral response functions were obtained from: https://www.nwpsaf.eu/site/software/rttov/download/coefficients/spectral-response-functions/#visir (accessed on 10 April 2023).

Conflicts of Interest: The authors declare no conflicts of interest.

References

1. Shoko, C.; Mutanga, O.; Dube, T. Progress in the remote sensing of C3 and C4 grass species aboveground biomass over time and space. *ISPRS J. Photogramm. Remote Sens.* **2016**, *120*, 13–24. [CrossRef]
2. Morais, T.G.; Teixeira, R.F.; Figueiredo, M.; Domingos, T. The use of machine learning methods to estimate aboveground biomass of grasslands: A review. *Ecol. Indic.* **2021**, *130*, 108081. [CrossRef]
3. Fu, X.; Tang, C.; Zhang, X.; Fu, J.; Jiang, D. An improved indicator of simulated grassland production based on MODIS NDVI and GPP data: A case study in the Sichuan province, China. *Ecol. Indic.* **2014**, *40*, 102–108. [CrossRef]
4. Dongmei, L.; Feng, J.; Bo, L. Aboveground biomass production and soil moisture characteristics of different herb communities in the Loess Hilly-gully Region. *Sci. Soil Water Conserv.* **2014**, *12*, 33–37.
5. Anaya, J.A.; Chuvieco, E.; Palacios-Orueta, A. Aboveground biomass assessment in Colombia: A remote sensing approach. *For. Ecol. Manag.* **2009**, *257*, 1237–1246. [CrossRef]
6. Su, Y.; Guo, Q.; Xue, B.; Hu, T.; Alvarez, O.; Tao, S.; Fang, J. Spatial distribution of forest aboveground biomass in China: Estimation through combination of spaceborne lidar, optical imagery, and forest inventory data. *Remote Sens. Environ.* **2016**, *173*, 187–199. [CrossRef]
7. Deng, Y.; Wang, S.; Bai, X.; Luo, G.; Wu, L.; Chen, F.; Wang, J.; Li, Q.; Li, C.; Yang, Y. Spatiotemporal dynamics of soil moisture in the karst areas of China based on reanalysis and observations data. *J. Hydrol.* **2020**, *585*, 124744. [CrossRef]
8. Gong, S.; Wang, S.; Bai, X.; Luo, G.; Wu, L.; Chen, F.; Qian, Q.; Xiao, J.; Zeng, C. Response of the weathering carbon sink in terrestrial rocks to climate variables and ecological restoration in China. *Sci. Total Environ.* **2021**, *750*, 141525. [CrossRef]
9. Shen, G.; Yang, X.; Jin, Y.; Luo, S.; Xu, B.; Zhou, Q. Land use changes in the Zoige Plateau based on the object-oriented method and their effects on landscape patterns. *Remote Sens.* **2019**, *12*, 14. [CrossRef]
10. Yang, Y.; Fang, J.; Pan, Y.; Ji, C. Aboveground biomass in Tibetan grasslands. *J. Arid Environ.* **2009**, *73*, 91–95. [CrossRef]
11. Yin, G.; Li, A.; Wu, C.; Wang, J.; Xie, Q.; Zhang, Z.; Nan, X.; Jin, H.; Bian, J.; Lei, G. Seamless upscaling of the field-measured grassland aboveground biomass based on gaussian process regression and gap-filled landsat 8 OLI reflectance. *ISPRS Int. J. Geo-Inf.* **2018**, *7*, 242. [CrossRef]
12. Yu, H.; Wu, Y.; Niu, L.; Chai, Y.; Feng, Q.; Wang, W.; Liang, T. A method to avoid spatial overfitting in estimation of grassland above-ground biomass on the Tibetan Plateau. *Ecol. Indic.* **2021**, *125*, 107450. [CrossRef]
13. Ge, J.; Hou, M.; Liang, T.; Feng, Q.; Meng, X.; Liu, J.; Bao, X.; Gao, H. Spatiotemporal dynamics of grassland aboveground biomass and its driving factors in North China over the past 20 years. *Sci. Total Environ.* **2022**, *826*, 154226. [CrossRef]
14. Sinha, S.; Jeganathan, C.; Sharma, L.K.; Nathawat, M.S. A review of radar remote sensing for biomass estimation. *Int. J. Environ. Sci. Technol.* **2015**, *12*, 1779–1792. [CrossRef]
15. Meng, B.; Liang, T.; Yi, S.; Yin, J.; Cui, X.; Ge, J.; Hou, M.; Lv, Y.; Sun, Y. Modeling alpine grassland above ground biomass based on remote sensing data and machine learning algorithm: A case study in east of the Tibetan Plateau, China. *IEEE J. Sel. Top. Appl. Earth Obs. Remote Sens.* **2020**, *13*, 2986–2995. [CrossRef]
16. Xie, Y.; Sha, Z.; Yu, M.; Bai, Y.; Zhang, L. A comparison of two models with Landsat data for estimating above ground grassland biomass in Inner Mongolia, China. *Ecol. Model.* **2009**, *220*, 1810–1818. [CrossRef]

17. Nordberg, M.-L.; Evertson, J. Monitoring change in mountainous dry-heath vegetation at a regional ScaleUsing multitemporal landsat TM data. *AMBIO J. Hum. Environ.* **2003**, *32*, 502–509. [CrossRef]

18. Barrachina, M.; Cristóbal, J.; Tulla, A.F. Estimating above-ground biomass on mountain meadows and pastures through remote sensing. *Int. J. Appl. Earth Obs. Geoinf.* **2015**, *38*, 184–192. [CrossRef]

19. Chen, Q.; Laurin, G.V.; Valentini, R. Uncertainty of remotely sensed aboveground biomass over an African tropical forest: Propagating errors from trees to plots to pixels. *Remote Sens. Environ.* **2015**, *160*, 134–143. [CrossRef]

20. Quan, X.; He, B.; Yebra, M.; Yin, C.; Liao, Z.; Zhang, X.; Li, X. A radiative transfer model-based method for the estimation of grassland aboveground biomass. *Int. J. Appl. Earth Obs. Geoinf.* **2017**, *54*, 159–168. [CrossRef]

21. Jiang, Y.; Tao, J.; Huang, Y.; Zhu, J.; Tian, L.; Zhang, Y. The spatial pattern of grassland aboveground biomass on Xizang Plateau and its climatic controls. *J. Plant Ecol.* **2015**, *8*, 30–40. [CrossRef]

22. Li, F.; Zeng, Y.; Luo, J.; Ma, R.; Wu, B. Modeling grassland aboveground biomass using a pure vegetation index. *Ecol. Indic.* **2016**, *62*, 279–288. [CrossRef]

23. Rasche, F.; Marhan, S.; Berner, D.; Keil, D.; Kandeler, E.; Cadisch, G. midDRIFTS-based partial least square regression analysis allows predicting microbial biomass, enzyme activities and 16S rRNA gene abundance in soils of temperate grasslands. *Soil Biol. Biochem.* **2013**, *57*, 504–512. [CrossRef]

24. Otgonbayar, M.; Atzberger, C.; Chambers, J.; Damdinsuren, A. Mapping pasture biomass in Mongolia using partial least squares, random forest regression and Landsat 8 imagery. *Int. J. Remote Sens.* **2019**, *40*, 3204–3226. [CrossRef]

25. Zeng, N.; Ren, X.; He, H.; Zhang, L.; Li, P.; Niu, Z. Estimating the grassland aboveground biomass in the Three-River Headwater Region of China using machine learning and Bayesian model averaging. *Environ. Res. Lett.* **2021**, *16*, 114020. [CrossRef]

26. Guo, R.; Fu, S.; Hou, M.-j.; Liu, J.; Miao, C.-l.; Meng, X.-y.; Feng, Q.-s.; He, J.-s.; Qiao, D.-w.; Liang, T.-g. Remote sensing retrieval of nature grassland biomass in Menyuan County, Qinghai Province experimental area based on Sentinel-2 data. *Acta Prataculturae Sin.* **2023**, *32*, 15.

27. Yang, S.; Feng, Q.; Liang, T.; Liu, B.; Zhang, W.; Xie, H. Modeling grassland above-ground biomass based on artificial neural network and remote sensing in the Three-River Headwaters Region. *Remote Sens. Environ.* **2018**, *204*, 448–455. [CrossRef]

28. Vamvakoulas, C.; Alexandris, S.; Argyrokastritis, I. Dry above ground biomass for a soybean crop using an empirical model in Greece. *Energies* **2020**, *13*, 201. [CrossRef]

29. Zeng, N.; Ren, X.; He, H.; Zhang, L.; Zhao, D.; Ge, R.; Li, P.; Niu, Z. Estimating grassland aboveground biomass on the Tibetan Plateau using a random forest algorithm. *Ecol. Indic.* **2019**, *102*, 479–487. [CrossRef]

30. Liu, W.; Xu, C.; Zhang, Z.; De Boeck, H.; Wang, Y.; Zhang, L.; Xu, X.; Zhang, C.; Chen, G.; Xu, C. Machine learning-based grassland aboveground biomass estimation and its response to climate variation in Southwest China. *Front. Ecol. Evol.* **2023**, *11*, 1146850. [CrossRef]

31. Darvishzadeh, R.; Skidmore, A.; Schlerf, M.; Atzberger, C. Inversion of a radiative transfer model for estimating vegetation LAI and chlorophyll in a heterogeneous grassland. *Remote Sens. Environ.* **2008**, *112*, 2592–2604. [CrossRef]

32. He, L.; Li, A.; Yin, G.; Nan, X.; Bian, J. Retrieval of grassland aboveground biomass through inversion of the PROSAIL model with MODIS imagery. *Remote Sens.* **2019**, *11*, 1597. [CrossRef]

33. Punalekar, S.M.; Verhoef, A.; Quaife, T.; Humphries, D.; Bermingham, L.; Reynolds, C. Application of Sentinel-2A data for pasture biomass monitoring using a physically based radiative transfer model. *Remote Sens. Environ.* **2018**, *218*, 207–220. [CrossRef]

34. Si, Y.; Schlerf, M.; Zurita-Milla, R.; Skidmore, A.; Wang, T. Mapping spatio-temporal variation of grassland quantity and quality using MERIS data and the PROSAIL model. *Remote Sens. Environ.* **2012**, *121*, 415–425. [CrossRef]

35. Duan, S.-B.; Li, Z.-L.; Wu, H.; Tang, B.-H.; Ma, L.; Zhao, E.; Li, C. Inversion of the PROSAIL model to estimate leaf area index of maize, potato, and sunflower fields from unmanned aerial vehicle hyperspectral data. *Int. J. Appl. Earth Obs. Geoinf.* **2014**, *26*, 12–20. [CrossRef]

36. Adeluyi, O.; Harris, A.; Verrelst, J.; Foster, T.; Clay, G.D. Estimating the phenological dynamics of irrigated rice leaf area index using the combination of PROSAIL and Gaussian Process Regression. *Int. J. Appl. Earth Obs. Geoinf.* **2021**, *102*, 102454. [CrossRef]

37. Pampanoni, V.; Laneve, G.; Santilli, G. Evaluating Sentinel-3 Viability for Vegetation Canopy Monitoring and Fuel Moisture Content Estimation. In Proceedings of the IGARSS 2022–2022 IEEE International Geoscience and Remote Sensing Symposium, Kuala Lumpur, Malaysia, 17–22 July 2022; IEEE: Piscataway, NJ, USA, 2022; pp. 5634–5637.

38. Casas, A.; Riaño, D.; Ustin, S.; Dennison, P.; Salas, J. Estimation of water-related biochemical and biophysical vegetation properties using multitemporal airborne hyperspectral data and its comparison to MODIS spectral response. *Remote Sens. Environ.* **2014**, *148*, 28–41. [CrossRef]

39. Rivera, J.P.; Verrelst, J.; Leonenko, G.; Moreno, J. Multiple cost functions and regularization options for improved retrieval of leaf chlorophyll content and LAI through inversion of the PROSAIL model. *Remote Sens.* **2013**, *5*, 3280–3304. [CrossRef]

40. Wan, L.; Zhang, J.; Dong, X.; Du, X.; Zhu, J.; Sun, D.; Liu, Y.; He, Y.; Cen, H. Unmanned aerial vehicle-based field phenotyping of crop biomass using growth traits retrieved from PROSAIL model. *Comput. Electron. Agric.* **2021**, *187*, 106304. [CrossRef]

41. Jiao, Q.; Sun, Q.; Zhang, B.; Huang, W.; Ye, H.; Zhang, Z.; Zhang, X.; Qian, B. A random forest algorithm for retrieving canopy chlorophyll content of wheat and soybean trained with PROSAIL simulations using adjusted average leaf angle. *Remote Sens.* **2021**, *14*, 98. [CrossRef]

42. Boser, B.E.; Guyon, I.M.; Vapnik, V.N. A training algorithm for optimal margin classifiers. In Proceedings of the Fifth Annual Workshop on Computational Learning Theory, Pittsburgh, PA, USA, 27–29 July 1992; pp. 144–152.

43. Deb, D.; Deb, S.; Chakraborty, D.; Singh, J.; Singh, A.K.; Dutta, P.; Choudhury, A. Aboveground biomass estimation of an agro-pastoral ecology in semi-arid Bundelkhand region of India from Landsat data: A comparison of support vector machine and traditional regression models. *Geocarto Int.* **2022**, *37*, 1043–1058. [CrossRef]

44. Durbha, S.S.; King, R.L.; Younan, N.H. Support vector machines regression for retrieval of leaf area index from multiangle imaging spectroradiometer. *Remote Sens. Environ.* **2007**, *107*, 348–361. [CrossRef]

45. Liang, D.; Guan, Q.; Huang, W.; Huang, L.; Yang, G. Remote sensing inversion of leaf area index based on support vector machine regression in winter wheat. *Trans. Chin. Soc. Agric. Eng.* **2013**, *29*, 117–123.

46. Sawut, R.; Li, Y.; Liu, Y.; Kasim, N.; Hasan, U.; Tao, W. Retrieval of betalain contents based on the coupling of radiative transfer model and SVM model. *Int. J. Appl. Earth Obs. Geoinf.* **2021**, *100*, 102340. [CrossRef]

47. Hou, M.; Ge, J.; Gao, J.; Meng, B.; Li, Y.; Yin, J.; Liu, J.; Feng, Q.; Liang, T. Ecological risk assessment and impact factor analysis of alpine wetland ecosystem based on LUCC and boosted regression tree on the Zoige Plateau, China. *Remote Sens.* **2020**, *12*, 368. [CrossRef]

48. Zhang, Y.; Wang, G.; Wang, Y. Changes in alpine wetland ecosystems of the Qinghai–Tibetan plateau from 1967 to 2004. *Environ. Monit. Assess.* **2011**, *180*, 189–199. [CrossRef]

49. Tripathi, R.; Sahoo, R.N.; Sehgal, V.K.; Tomar, R.; Chakraborty, D.; Nagarajan, S. Inversion of PROSAIL model for retrieval of plant biophysical parameters. *J. Indian Soc. Remote Sens.* **2012**, *40*, 19–28. [CrossRef]

50. Jacquemoud, S.; Baret, F. PROSPECT: A model of leaf optical properties spectra. *Remote Sens. Environ.* **1990**, *34*, 75–91. [CrossRef]

51. Verhoef, W. Light scattering by leaf layers with application to canopy reflectance modeling: The SAIL model. *Remote Sens. Environ.* **1984**, *16*, 125–141. [CrossRef]

52. Darvishzadeh, R.; Matkan, A.A.; Ahangar, A.D. Inversion of a radiative transfer model for estimation of rice canopy chlorophyll content using a lookup-table approach. *IEEE J. Sel. Top. Appl. Earth Obs. Remote Sens.* **2012**, *5*, 1222–1230. [CrossRef]

53. Kuusk, A. The hot spot effect in plant canopy reflectance. In *Photon-Vegetation Interactions: Applications in Optical Remote Sensing and Plant Ecology*; Springer: Berlin/Heidelberg, Germany, 1991; pp. 139–159.

54. Dimov, I.; Georgieva, R. Monte Carlo algorithms for evaluating Sobol'sensitivity indices. *Math. Comput. Simul.* **2010**, *81*, 506–514. [CrossRef]

55. Xu, M.; Liu, R.; Chen, J.M.; Liu, Y.; Shang, R.; Ju, W.; Wu, C.; Huang, W. Retrieving leaf chlorophyll content using a matrix-based vegetation index combination approach. *Remote Sens. Environ.* **2019**, *224*, 60–73. [CrossRef]

56. Feilhauer, H.; Schmid, T.; Faude, U.; Sanchez-Carrillo, S.; Cirujano, S. Are remotely sensed traits suitable for ecological analysis? A case study of long-term drought effects on leaf mass per area of wetland vegetation. *Ecol. Indic.* **2018**, *88*, 232–240. [CrossRef]

57. Liang, L.; Di, L.; Zhang, L.; Deng, M.; Qin, Z.; Zhao, S.; Lin, H. Estimation of crop LAI using hyperspectral vegetation indices and a hybrid inversion method. *Remote Sens. Environ.* **2015**, *165*, 123–134. [CrossRef]

58. Huang, J.; Ma, H.; Sedano, F.; Lewis, P.; Liang, S.; Wu, Q.; Su, W.; Zhang, X.; Zhu, D. Evaluation of regional estimates of winter wheat yield by assimilating three remotely sensed reflectance datasets into the coupled WOFOST–PROSAIL model. *Eur. J. Agron.* **2019**, *102*, 1–13. [CrossRef]

59. Li, X.; Mao, F.; Du, H.; Zhou, G.; Xu, X.; Han, N.; Sun, S.; Gao, G.; Chen, L. Assimilating leaf area index of three typical types of subtropical forest in China from MODIS time series data based on the integrated ensemble Kalman filter and PROSAIL model. *ISPRS J. Photogramm. Remote Sens.* **2017**, *126*, 68–78. [CrossRef]

60. Vapnik, V. *The Nature of Statistical Learning Theory*; Springer Science & Business Media: Berlin/Heidelberg, Germany, 1999.

61. Panahi, M.; Sadhasivam, N.; Pourghasemi, H.R.; Rezaie, F.; Lee, S. Spatial prediction of groundwater potential mapping based on convolutional neural network (CNN) and support vector regression (SVR). *J. Hydrol.* **2020**, *588*, 125033. [CrossRef]

62. Zhang, L.; Gao, H.; Zhang, X. Combining Radiative Transfer Model and Regression Algorithms for Estimating Aboveground Biomass of Grassland in West Ujimqin, China. *Remote Sens.* **2023**, *15*, 2918. [CrossRef]

63. Chen, J.; Yamamura, Y.; Hori, Y.; Shiyomi, M.; Yasuda, T.; Zhou, H.-k.; Li, Y.-n.; Tang, Y.-h. Small-scale species richness and its spatial variation in an alpine meadow on the Qinghai-Tibet Plateau. *Ecol. Res.* **2008**, *23*, 657–663. [CrossRef]

64. Wang, J.; Li, A.; Bian, J. Simulation of the grazing effects on grassland aboveground net primary production using DNDC model combined with time-series remote sensing data—A case study in Zoige Plateau, China. *Remote Sens.* **2016**, *8*, 168. [CrossRef]

65. Guo, H.-l.; Li, X.; Fu, Y.; Qiao, B.-j. High-resolution leaf area index inversion based on the Kernel Ridge Regression algorithm and PROSAIL model. *Acta Prataculturae Sin.* **2022**, *31*, 41.

66. Mo, X.-G.; Liu, W.; Meng, C.-C.; Hu, S.; Liu, S.-X.; Lin, Z.-H. Variations of forage yield and forage-livestock balance in grasslands over the Tibetan Pla-teau, China. *Ying Yong Sheng Tai Xue Bao = J. Appl. Ecol.* **2021**, *32*, 2415–2425.

67. Xie, J.; Wang, C.; Ma, D.; Chen, R.; Xie, Q.; Xu, B.; Zhao, W.; Yin, G. Generating spatiotemporally continuous grassland aboveground biomass on the tibetan plateau through PROSAIL model inversion on google earth engine. *IEEE Trans. Geosci. Remote Sens.* **2022**, *60*, 1–10. [CrossRef]

68. Baldridge, A.M.; Hook, S.J.; Grove, C.; Rivera, G. The ASTER spectral library version 2.0. *Remote Sens. Environ.* **2009**, *113*, 711–715. [CrossRef]